Study on the Influence of Al_2O_3 Diffusion Barrier Prepared by Atmospheric Plasma Spraying on the Interface Stability during the Preparation Process of Mo-Si-B/Nb-Si Based Alloy Coating System

Qingyan Hou[1] and Lei Jin[2,*]

[1]*Institute of Radiation Technology, Beijing Academy of Science and Technology, Beijing 100875, China*

[2]*Aviation Key Laboratory of Science and Technology on Advanced Surface Engineering, AVIC Manufacturing Technology Institute, Beijing 100024, China*

Abstract: The interdiffusion between Mo-Si-B coatings and Nb-Si based alloys during preparation and service at high temperatures remains a critical issue, which deteriorates the coating performance and embrittles the substrate. In this study, the atmospheric plasma spraying (APS) technology was adopted to prepare the Al_2O_3 diffusion barrier between the Mo-Si-B coating and the NB-Si-based alloy, and the influence of spark plasma sintering (SPS) pressure on the microstructure and mutual diffusion behavior of the diffusion barrier was systematically investigated. Microstructure analysis indicates that under the condition of 40 MPa and 1300ºC, the diffusion barrier remains dense and continuous, completely inhibiting the interdiffusion between the coating and the substrate. This work demonstrates, for the first time, the successful application of an APS-fabricated η- Al_2O_3 layer as an effective diffusion barrier during the SPS process, highlighting its potential for large-scale, low-cost protection of Nb-Si based alloys, with the caveat that its performance is critically dependent on the applied pressure during the preparation process.

Keywords: Atmosphere Plasma Spray (APS); Alumina Diffusion Barrier; Spark Plasma Sintering (SPS); Mo-Si-B Coating; Nb-Si Based Alloy.

1. INTRODUCTION

Nb-Si based alloys are promising candidates for next-generation high-temperature structural applications in aerospace and gas turbines owing to their high melting point and attractive strength-to-density ratio [1, 2]. However, their poor oxidation resistance above 1000ºC severely limits practical use [3]. To address this challenge, Mo-Si-B coatings have been extensively investigated as a protective system, capable of forming a continuous, protective SiO_2 or borosilicate glass scale upon exposure to high-temperature air [4].

A significant obstacle in applying these coatings is the severe interdiffusion that occurs between the coating and the Nb-Si substrate during both high-temperature processing and service [5]. This interdiffusion leads to the formation of brittle intermetallic phases (e.g., Nb_5Si_3, Mo_5Si_3), depletion of protective elements from the coating, and ultimately, the degradation of oxidation resistance and mechanical integrity of the system.

Our previous research has systematically documented this problem and explored solutions. In our earlier work, Mo–Si–B coatings fabricated by spark plasma sintering (SPS) experienced substantial interdiffusion with the substrate during both the coating process and subsequent static oxidation at 1250°C for 100 hours [6]. To address this issue, the introduction of a diffusion barrier has been demonstrated as an effective strategy to suppress interdiffusion between the coating and the substrate. In two subsequent studies, we successfully implemented this approach: an Al_2O_3 diffusion barrier was fabricated via plasma spray–physical vapor deposition (PS-PVD), which effectively mitigated interdiffusion during both coating deposition and static oxidation at 1250 °C[7]. Similarly, a TiN diffusion barrier deposited by magnetron sputtering also achieved significant suppression of interdiffusion in both cases [8].

While these vapor deposition techniques provide high-quality, dense barriers, they are associated with high equipment costs, low deposition rates, and limitations in coating complex geometries, which hinders their large-scale industrial application. Atmosphere Plasma Spraying (APS) offers a compelling alternative. It is a well-established, economical, and versatile technique capable of high deposition rates and coating large or complex components [9, 10]. Al_2O_3, a thermodynamically stable and diffusion-resistant ceramic, is a prime candidate material for such a barrier [11]. However, the typical as-sprayed APS coating possesses a structure with inherent microcracks and

*Address correspondence to this author at China Science and Technology on Power Beam Processes Laboratory, AVIC Manufacturing Technology Institute, Beijing, 100024, China; E-mail: 825620669@qq.com

E-ISSN: 3110-9780/25

porosity, which might compromise its effectiveness as a diffusion barrier. Furthermore, the stability and performance of an APS-fabricated Al_2O_3 barrier under the combined conditions—high temperature, pressure, and electrical discharge—of a subsequent SPS process have not been investigated.

This work bridges that gap. For the first time, we evaluate an atmospheric-plasma-sprayed η-Al_2O_3 diffusion barrier specifically for Mo-Si-B-coated Nb-Si-based alloys that must subsequently undergo spark-plasma sintering. Unlike our previous PS-PVD or magnetron-sputtered barriers, the present study focuses on the barrier's integrity and diffusion-mitigation performance under the simultaneous high-temperature, pressure and electrical-discharge conditions inherent to SPS. Elucidating the influence of SPS pressure on the APS coating microstructure provides a novel, cost-effective and scalable route toward robust protective coating systems for refractory alloys.

2. EXPERIMENTAL AND COMPUTATIONAL DETAILS

2.1. Coating Preparation

The Nb-Si based alloy used as the substrate material was prepared in-house[12]. The size of the Nb-Si base is 20 mm in diameter and 3 mm in thickness. Prior to deposition, the substrate surfaces were ground with 200-grit water-fed sandpaper to enhance coating adhesion. An Al_2O_3 diffusion barrier layer was deposited onto the substrate via atmospheric plasma spraying (APS) using an APS-3000 system. Spraying parameters were optimized to produce a dense barrier layer: a high-enthalpy plasma jet was generated at 35 kW (500 A, 70 V) with a powder feed rate of 45 g min^{-1} and a gas mixture of Ar (60 L/min) + H_2 (2 L/min) to ensure complete melting of the α-Al_2O_3 feedstock. A stand-off distance of 100 mm was selected to balance in-flight particle velocity and temperature, enabling adequate droplet spreading upon impact while minimizing excessive heat loss. This combination reduces unmelted particles and interlamellar porosity, thereby lowering overall coating porosity and improving barrier performance.

To mitigate potential detrimental effects on the mechanical properties of the system caused by excessive thickness and to facilitate consistent comparison with other types of diffusion barriers, the as-sprayed Al_2O_3 layer was ground down using 1500-grit sandpaper to achieve a flat and reduced-thickness barrier. Subsequently, the Mo-Si-B oxidation-resistant coating was applied on top of the Al_2O_3 barrier by SPS [10, 13]. For this step, the sample with the Al_2O_3 barrier and Mo-Si-B mixed powder were placed together into a graphite die and consolidated under two different SPS parameter sets to investigate the influence of processing conditions on interfacial stability:

Set A: Temperature of 1300 °C and pressure of 50 MPa.

Set B: Temperature of 1300 °C and pressure of 40 MPa.

2.2. Specimen Characterization

The as-sprayed Al_2O_3 coating was first characterized by X-ray diffraction (XRD) to determine its phase composition. The cross-sectional morphology, interfacial structure, and elemental distribution of the final Mo-Si-B/Al_2O_3/Nb-Si coating system were then examined using scanning electron microscopy (SEM) equipped with energy-dispersive X-ray spectroscopy (EDS).

3. RESULTS AND DISCUSSION

3.1. Microstructure of the Al_2O_3 Diffusion Barrier Coating Prepared by APS

Figure **1** presents the XRD pattern of the as-deposited Al_2O_3 coating produced by APS. The coating is predominantly composed of the η-Al_2O_3 phase[14], with minor diffraction peaks corresponding to α-Al_2O_3 [10, 15]. This phase composition is typical for plasma-sprayed alumina. The formation and retention of the metastable η-phase can be attributed to the complete melting of the feedstock powder in the high-temperature plasma jet and its subsequent rapid solidification on the substrate—a characteristic non-equilibrium process. Although the α-Al_2O_3 polymorph is thermodynamically more stable and known for its superior chemical inertness and lower oxygen diffusivity, the effectiveness of the as-sprayed η-Al_2O_3 as an initial diffusion barrier is contingent upon its structural stability during the subsequent SPS cycle.

Figure **2** displays the cross-sectional morphology of the as-deposited Al_2O_3 coating fabricated by APS. The coating thickness is around 300 μm. Characteristic defects inherent to the APS process, including partially melted particles and interlamellar microcracks, are evident in the microstructure [16]. The presence of

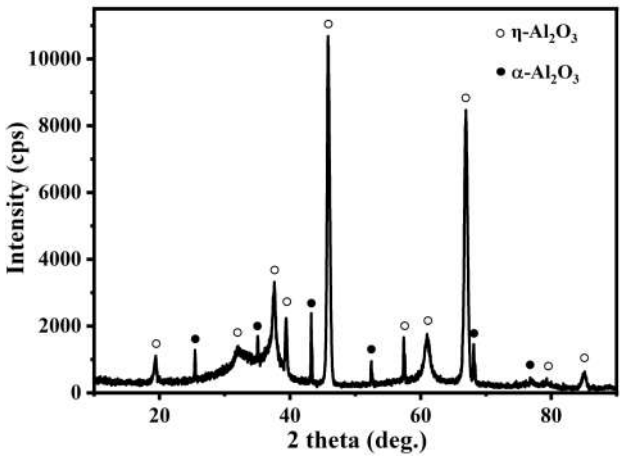

Figure 1: XRD image of Al_2O_3 layer by plasma spraying.

these features results in a lower overall density compared to coatings produced by PVD techniques [17-19].

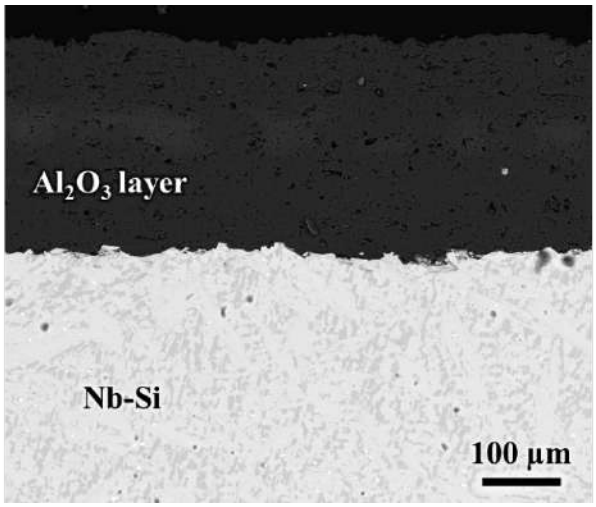

Figure 2: Cross-section image of Al_2O_3 layer by plasma spraying.

A critical and innovative step in this study involved the mechanical thinning of the as-sprayed 300 μm APS-Al_2O_3 coating to a significantly reduced thickness. This post-deposition treatment was not arbitrary but was driven by the following crucial technical rationale:

Mitigation of Residual Stresses and Enhancement of Interfacial Adhesion: The significant mismatch in the coefficients of thermal expansion (CTE) between the Al_2O_3 ceramic and the Nb-Si metallic substrate inevitably leads to the development of substantial residual stresses within the thick (300 μm) coating upon cooling from the high APS deposition temperature [20]. These stresses can compromise interfacial adhesion and promote coating delamination or cracking during subsequent processing. Reducing the coating thickness effectively diminishes the total strain energy stored in the ceramic layer, thereby significantly lowering the driving force for failure and improving the thermo-mechanical stability of the interface.

Compatibility with the SPS Consolidation Environment: The SPS process subjects the sample to simultaneous high temperature and pressure (40-50 MPa). A thick, inherently flawed brittle ceramic layer is highly susceptible to crushing or shear fracture under these conditions. In contrast, a thin layer exhibits superior mechanical compliance at the sintering temperature. It can better accommodate the applied pressure by embedding between the substrate and the top-coating powder, enabling cooperative deformation and enhancing its likelihood of surviving the SPS cycle with its structural integrity intact.

Optimization of Interfacial Contact for SPS: The inherently rough surface of an as-sprayed APS coating would result in poor and non-uniform contact with the Mo-Si-B powder during SPS. This could lead to inadequate current distribution, localized insufficient sintering, and the formation of voids at the interface. Precision grinding creates a smooth and planar surface, ensuring excellent physical contact with the overlying powder. This is a prerequisite for uniform pressure distribution, efficient Joule heating, and the subsequent formation of a dense, well-bonded Mo-Si-B top coating.

Strategic Balance Between Barrier Efficacy and Process Robustness: While a thicker barrier theoretically provides a longer diffusion path, its primary function is to be "impervious" rather than merely "retarding." Once a barrier is dense and continuous, its effectiveness is not substantially enhanced by further increasing its thickness beyond a critical value, as evidenced by the successful use of several micron PVD barriers in prior art. The selected thickness far exceeds the minimum requirement for effective diffusion blockage while proactively mitigating the risks (stress, fracture) associated with excessively thick ceramic layers, thus striking an optimal balance between performance, reliability, and processing practicality.

In summary, the strategy of "thick deposition followed by precision thinning" leverages the high

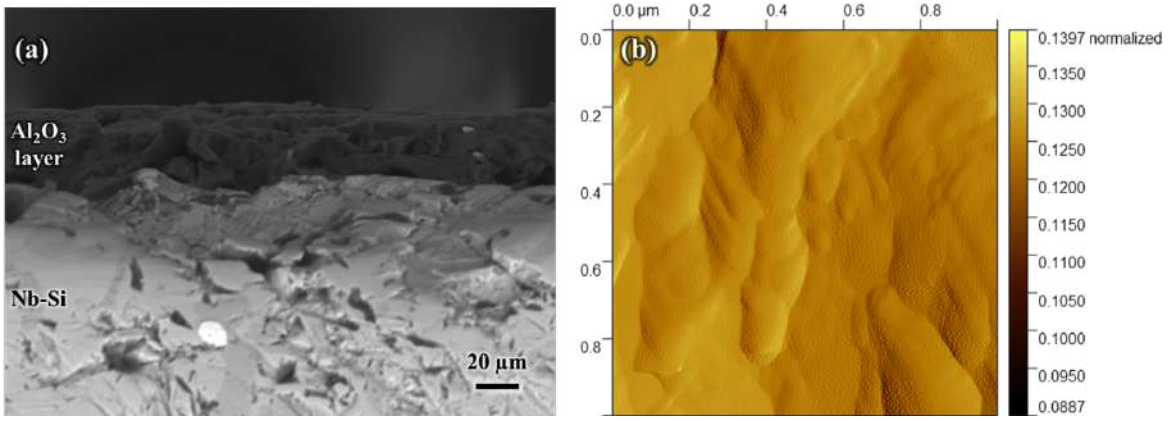

Figure 3: (**a**) Cross-sectional SEM micrograph of the ground APS-Al_2O_3 diffusion barrier; (**b**) AFM surface topography (1 μm × 1 μm scan area).

deposition rate of APS while circumventing its microstructural shortcomings. This hybrid approach yields a high-performance diffusion barrier that is not only functionally adequate but also specifically engineered to withstand the rigors of the subsequent SPS consolidation process. Figure **3a** shows a representative cross-sectional SEM image of the ground APS-Al_2O_3 barrier; the uniform thickness is around 30 μm. Figure **3b** presents the corresponding AFM surface scan (1 μm × 1 μm), yielding Sa = 0.048 μm. These values ensure intimate interfacial contact for reliable Joule heating and pressure transmission during subsequent SPS.

3.2. The Influence of SPS Pressure on the Interfacial Stability of Mo-Si-B/Al_2O_3/Nb-Si Coating System

3.2.1. Interface Structure Under a Pressure of 50 MPa

Figure **4** presents the cross-sectional morphology of the sample consolidated by SPS at 1300 °C and 50 MPa. As shown in Fig. **4a**, the Al_2O_3 diffusion barrier, although macroscopically retaining a layered morphology with a thickness of approximately 12 μm, suffers from severe loss of continuity, exhibiting obvious fragmentation and cracking. The coating-substrate interface exhibits significant irregularity. Localized concave regions, where the substrate surface appears depressed, are also observed, as highlighted in the blue box. As shown in Fig. **4b**, at those fracture sites, the overlying Mo–Si–B coating comes into direct contact with the underlying Nb–Si substrate, establishing continuous "diffusion channels" through the barrier layer.

Figure **5** displays the corresponding EDS elemental mapping results for the region detailed in Fig. **4b**, which substantiates the microstructural observations. In areas where the Al_2O_3 layer is fractured, Si from the Mo–Si–B coating is clearly seen penetrating toward the Nb–Si substrate through the cracks. Concurrently, elements such as Nb, Ti, and Cr from the substrate diffuse in the opposite direction into the coating, accumulating noticeably within the fractured regions of the alumina layer. This elemental interpenetration resembles the phenomenon previously observed in systems without a diffusion barrier.

A notable finding is the presence of subtle and discontinuous interdiffusion zones (IDZs) at the interfaces between the Al_2O_3 fragments and the Mo–Si–B coating. These IDZs terminate where the Al_2O_3 layer remains continuous and reappear only at the fracture sites, indicating that the intact portions of the Al_2O_3 barrier still effectively hinder the diffusion of Si. In contrast, a more pronounced and continuous IDZ, appearing as a distinct dark grey layer, is formed at the interface between the Al_2O_3 fragments and the Nb–Si substrate. EDS analysis identifies this layer as being rich in Ti.

Furthermore, the substrate adjacent to the interface exhibits intermittent bright white regions, which EDS mapping confirms are Hf-rich zones. This Hf enrichment is attributed to the substantial out-diffusion of Nb, Ti, and Cr from the substrate near the interface into the coating. The consequent depletion of these faster-diffusing elements leads to the relative enrichment of the slower-diffusing Hf within the substrate, manifesting as the observed bright contrast.

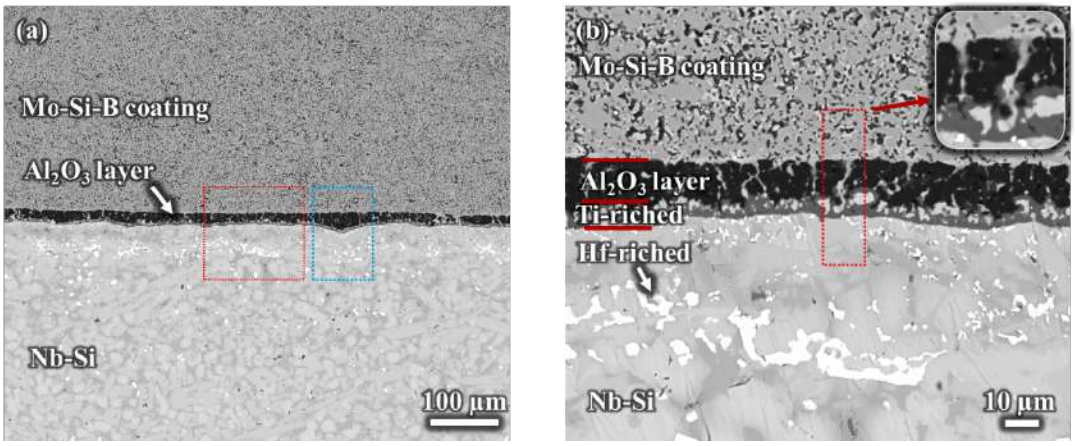

Figure 4: Cross-sectional SEM images of the multilayer structure (Mo-Si-B coating / Al_2O_3 interlayer / substrate) fabricated by SPS at 1300 °C and 50 MPa: (**a**) overall microstructure, and (**b**) a higher-magnification view of the coating-substrate interface.

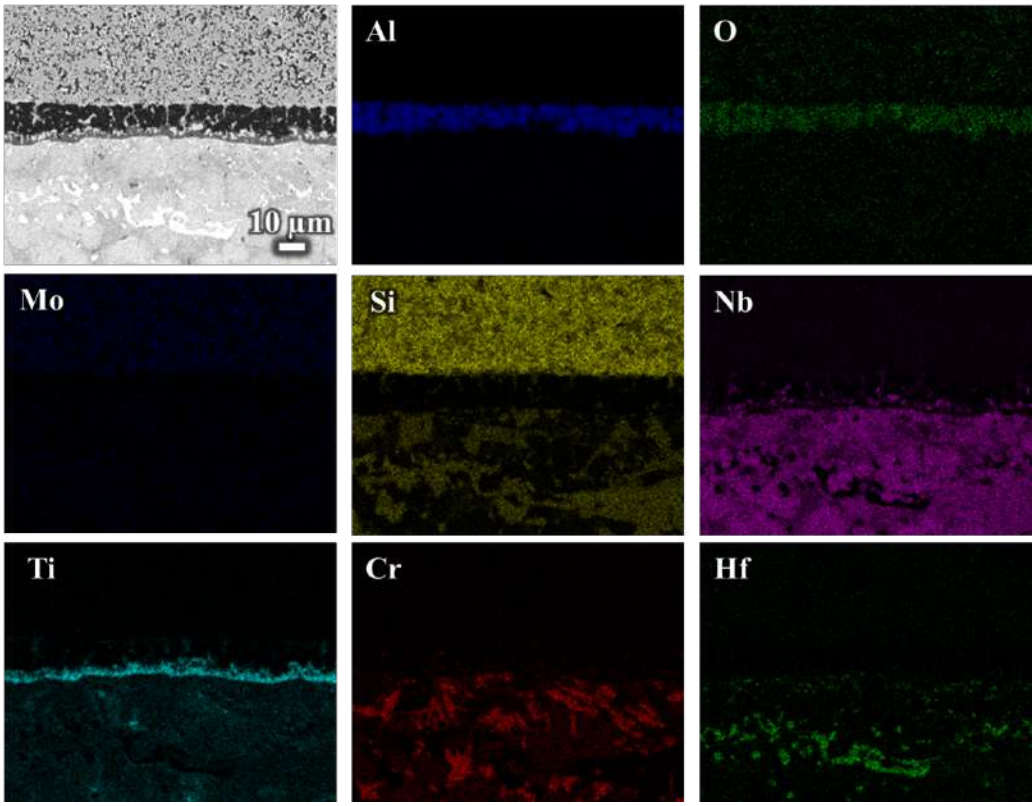

Figure 5: EDS elemental maps of the Mo–Si–B/Al_2O_3 coating system sintered at 1300 °C and 50 MPa, showing the elemental distribution across the interdiffusion zones (IDZs) formed at the interfaces.

3.2.2. Interface Structure under a Pressure of 40 MPa

Figure **6** and **7** displays the cross-sectional morphology and corresponding elemental distribution of the sample fabricated via SPS at 1300 °C and 40 MPa. The SEM image reveals that the Al_2O_3 diffusion barrier, situated between the Mo-Si-B coating and the Nb-Si substrate, exhibits a densely packed and continuous morphology despite the presence of some minor pores. The barrier maintains a uniform thickness, ranging approximately between 25 and 35 μm. The overall coating system presents a well-defined triple-layer architecture of "Mo-Si-B / Al_2O_3 / Nb-Si". The interfaces between these distinct layers are sharp, and the bonding appears sound, with no observable cracks or the formation of an IDZ. An EDS line-scan (Figure **6b**) across the 40 MPa specimen shows sharp compositional transitions at both interfaces, with no

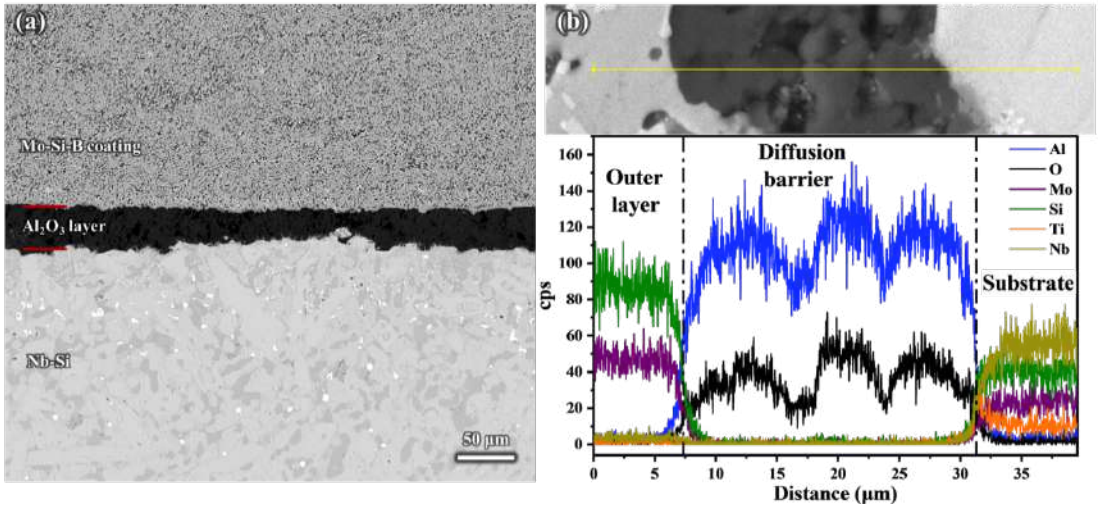

Figure 6: (a) Cross-sectional SEM image and (b) EDS line-scan of the multilayer structure (Mo-Si-B coating / Al_2O_3 interlayer / substrate) fabricated by SPS at 1300 °C and 40 MPa.

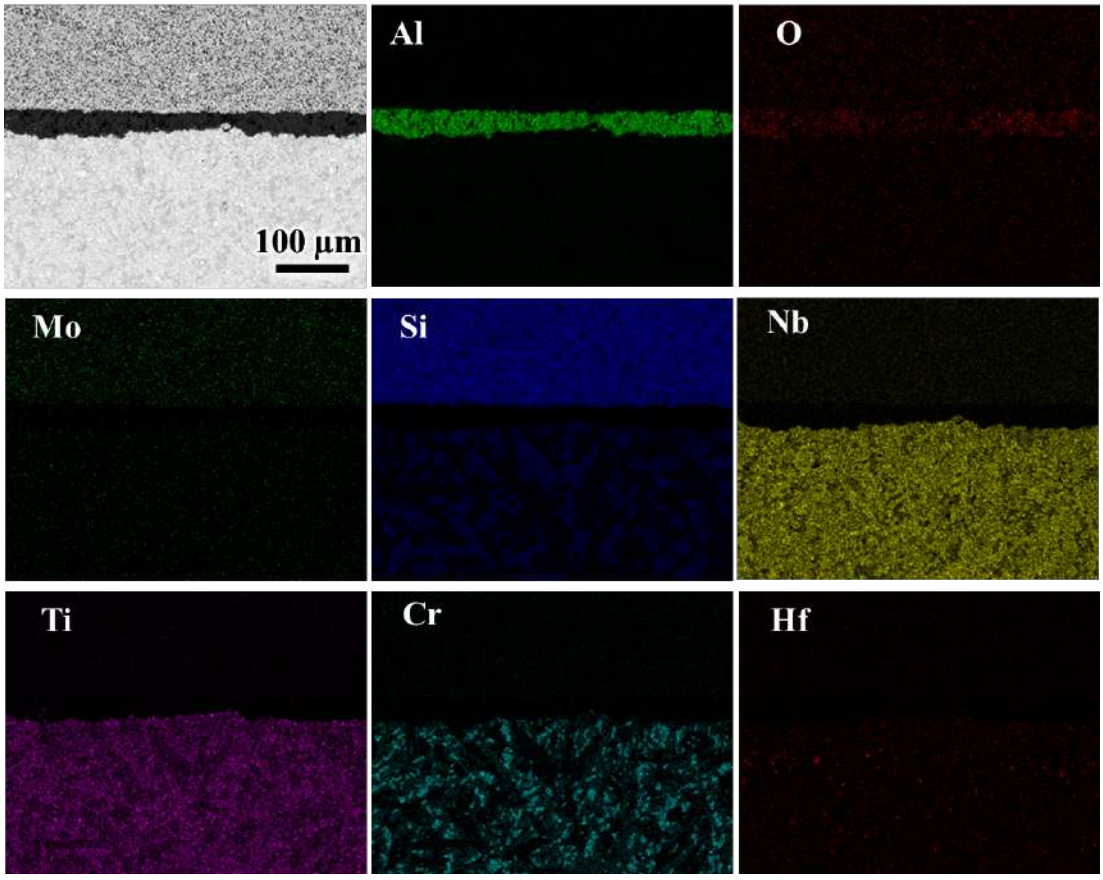

Figure 7: EDS elemental maps of the Mo–Si–B/Al_2O_3 coating system sintered at 1300 °C and 40 MP.

measurable Mo, Nb or Si penetration into the barrier, confirming the absence of detectable interdiffusion.

The EDS elemental mapping provides critical insight. Signals from Al and O are predominantly and clearly concentrated within the central barrier layer. Elements representative of the Mo-Si-B coating (Mo, Si) and those from the Nb-Si substrate (Nb, Ti, Cr and Hf) are effectively separated by the Al_2O_3 layer. At both the Mo-Si-B/Al_2O_3 and Al_2O_3/Nb-Si interfaces, the elemental distributions show steep gradients, with no detectable cross-interface interdiffusion. This confirms

that the optimized, approximately 30 μm thick APS-deposited η-Al_2O_3 barrier faithfully fulfilled its function under the applied SPS conditions of 1300 °C and 40 MPa, thereby effectively impeding elemental interdiffusion between the coating and substrate under high temperature and pressure.

These results underscore that the pressure applied during the SPS process is a critical parameter determining the performance of the APS-fabricated Al_2O_3 diffusion barrier. At 40 MPa, the ground and densified η-Al_2O_3 layer possessed adequate mechanical strength to withstand the coupled thermal and mechanical loads, with the applied stress remaining below the critical threshold for fracture. Its continuity and density were the keystones to its success, providing a physically impermeable wall against atomic interdiffusion at 1300°C. Conversely, the barrier fracture observed at 50 MPa is attributed to the inherent brittleness of the ceramic, where the higher pressure induced severe stress concentrations at micro-defects, ultimately exceeding the material's fracture strength.

CONCLUSIONS

Based on the systematic investigation conducted in this study, it can be concluded that the η-Al_2O_3 coating prepared by APS, after strategic post-deposition mechanical thinning from 300 μm to approximately 25-35 μm, successfully functions as an effective diffusion barrier between the Mo-Si-B coating and Nb-Si based alloy during the SPS process. The post-spray thinning treatment proved crucial for mitigating residual thermal stresses, improving interfacial adhesion, and ensuring compatibility with the subsequent SPS consolidation environment. The applied pressure during SPS emerges as the decisive parameter determining the barrier's efficacy. Under optimal conditions of 1300 °C and 40 MPa, the Al_2O_3 layer maintains perfect structural integrity, appearing as a continuous and dense layer that completely prevents any detectable interdiffusion between the coating and substrate, as unequivocally demonstrated by the sharp interfacial boundaries and absence of elemental interpenetration in EDS mapping. In contrast, when subjected to a higher pressure of 50 MPa, the barrier suffers mechanical fracture, forming through-thickness cracks that serve as rapid diffusion channels, leading to significant elemental interdiffusion and the formation of distinct interdiffusion zones, particularly at the barrier/substrate interface. This work establishes, for the first time, the successful integration of APS as a cost-effective fabrication route for diffusion barriers within multilayer coating systems for refractory alloy protection, while fundamentally highlighting the critical role of consolidation pressure - a previously overlooked parameter - in determining the performance of thermally sprayed ceramic barriers during SPS processing. The findings provide both a scientifically significant understanding and a practical, scalable strategy for developing robust protective coating systems.

ACKNOWLEDGEMENT

This project is supported by the Reform and Development Project of BJAST (25CB007-06).

REFERENCES

[1] Bewlay BP, Jackson MR, Zhao JC, Subramanian PR. A Review of Very-High-Temperature Nb-Silicide-Based Composites. Metallurgical and Materials Transactions a-Physical Metallurgy and Materials Science 2003; 34a: 2043-2052. http://doi.org/10.1007/s11661-003-0269-8

[2] Bewlay BP, Jackson MR, Zhao JC, Subramanian PR, Mendiratta MG, Lewandowski JJ, Ultrahigh-Temperature Nb-Silicide-Based Composites. MRS Bull 2011; 28: 646-653. http://doi.org/10.1557/mrs2003.192

[3] Geng J, Tsakiropoulos P. A Study of the Microstructures and Oxidation of Nb–Si–Cr–Al–Mo In Situ Composites Alloyed with Ti, Hf and Sn. Intermetallics 2007; 15: 382-395. http://doi.org/10.1016/j.intermet.2006.08.016

[4] Alam MZ, Venkataraman B, Sarma B, Das DK. $MoSi_2$ Coating on Mo Substrate for Short-term Oxidation Protection in Air. Journal of Alloys Compounds 2009; 487: 335-340.

[5] Wen SH, Sha JB. Isothermal and cyclic oxidation behaviours of $MoSi_2$ with additions of B at 1250 ° C prepared by spark plasma sintering. Mater Charact 2018; 139: 134-143. http://doi.org/10.1016/j.matchar.2018.02.037

[6] Hou QY, Li MF, Shao W, Zhou CG. Oxidation and interdiffusion behavior of Mo-Si-B coating on Nb-Si based alloy prepared by spark plasma sintering. Corros Sci 2020; 169. http://doi.org/ARTN10863810.1016/j.corsci.2020.108638

[7] Hou Q, Shao W, Li M, Zhou C. Interdiffusion behavior of Mo-Si-B/Al_2O_3 composite coating on Nb-Si based alloy. Surf Coat Technol 2020; 401. http://doi.org/10.1016/j.surfcoat.2020.126243

[8] Hou Q, Li M, Chen Z, Zhou C. Effect of TiN diffusion barrier on interdiffusion between Mo–Si–B coating and Nb–Si based alloy. Materials Chemistry Physics and Chemistry of Glasses 2025; 337.

[9] Jin L, Yu Q, Ni L, Zhou C. Microstructure and Thermal Properties of Nanostructured 8 wt.% CeO Doped YSZ Coatings Prepared by Atmospheric Plasma Spraying. J Therm Spray Technol 2012; 21: 928-934

[10] Gao Y, Jie M, Liu Y. Mechanical Properties of Al_2O_3 Ceramic Coatings Prepared by Plasma Spraying on Magnesium Alloy. Surf Coat Technol 2017; 315: 214-219. http://doi.org/10.1016/j.surfcoat.2017.02.026

[11] Deng W, Li S, Hou G, Liu X, Zhao X, An Y, Zhou H, Chen J. Comparative study on wear behavior of plasma sprayed Al_2O_3 coatings sliding against different counterparts. Ceram Int 2017; 43: 6976-6986. http://doi.org/10.1016/j.ceramint.2017.02.122

[12] Wen SH, Zhou CG, Sha JB. Microstructural evolution and oxidation behaviour of Mo-Si-B coatings on an Nb-16Si-22Ti-7Cr-2Al-2Hf alloy at 1250 ° C prepared by spark plasma sintering. Surf Coat Technol 2018; 352: 320-329. http://doi.org/10.1016/j.surfcoat.2018.08.027

[13] Wen SH, Zhou CG, Sha JB. Improvement of Oxidation Resistance of a Mo-62Si-5B (at.%) Alloy at 1250 °C and 1350 °C via an In Situ Pre-Formed SiO_2 Fabricated by Spark Plasma Sintering. Corros Sci 2017; 127: 175-185. http://doi.org/10.1016/j.corsci.2017.08.019

[14] Igel J, Scheld WS, Mack DE, Guillon O, Vaßen R. Lifetime Extension of Atmospheric and Suspension Plasma-Sprayed Thermal Barrier Coatings in Burner Rig Tests by Pre-Oxidizing the CoNiCrAlY Bond Coats. Coatings 2024; 14: 793

[15] Xu Y-X, Chirol M, Li C-J, Vardelle A. Formation of Al_2O_3 Diffusion Barrier in Cold-Sprayed NiCoCrAlY/Ni Multi-Layered Coatings on 304SS Substrate. Surf Coat Technol 2016; 307: 603-609. http://doi.org/10.1016/j.surfcoat.2016.09.058

[16] Michalak M, Łatka L, Sokołowski P, Niemiec A, Ambroziak A. The Microstructure and Selected Mechanical Properties of Al_2O_3 + 13 wt % TiO_2 Plasma Sprayed Coatings. Welding 2020; 10: 173.

[17] Cai F, Huang X, Yang Q, Nagy D. Tribological Behaviors of Titanium Nitride- and Chromium-Nitride-Based Physical Vapor Deposition Coating Systems. Journal of Engineering for Gas Turbines and Power 2012; 134. http://doi.org/10.1115/1.4007168

[18] Cremer R, Witthaut M, Reichert K, Neuschütz D. Surface and Interface Analysis of PVD Al-O-N and γ-Al_2O_3 Diffusion Barriers, Fresenius. Journal of Analytical Chemistry 1999; 365: 158-162. http://doi.org/10.1007/s002160051464

[19] Liang T, Guo H, Peng H, Gong S. Cyclic Oxidation Behavior of an EB-PVD CoCrAlY Coating Influenced by Substrate/coating Interdiffusion. Chinese Journal of Aeronautics 2012; 25: 796-803. http://doi.org/10.1016/s1000-9361(11)60447-0

[20] Shang CH, van Heerden D, Gavens AJ, Weihs TP. An X-ray Study of Residual Stresses and Bending Stresses in Free-Standing Nb/Nb_5Si_3 Microlaminates. Acta Mater 2000; 48: 3533-3543. http://doi.org/10.1016/S1359-6454(00)00125-7

Received on 12-10-2025 Accepted on 15-11-2025 Published on 28-11-2025

https://doi.org/10.66000/3110-9780.2025.01.04